

# M-PERC: A New Satellite Microwave-Based Model to Diagnose the Onset of Tropical Cyclone Eyewall Replacement Cycles

JAMES P. KOSSIN<sup>a,b,c</sup>, DERRICK C. HERNDON<sup>d</sup>, ANTHONY J. WIMMERS<sup>d</sup>, XI GUO<sup>d,e</sup> AND ERIC S. BLAKE<sup>f</sup>

<sup>a</sup> *The Climate Service (an S&P Global company), Madison, Wisconsin*

<sup>b</sup> *University of Wisconsin–Madison, Madison, Wisconsin*

<sup>c</sup> *Climate Science and Services Division, NOAA/National Centers for Environmental Information, Asheville, North Carolina*

<sup>d</sup> *Cooperative Institute for Meteorological Satellite Studies, Madison, Wisconsin*

<sup>e</sup> *Jiangsu Meteorological Observatory, Nanjing, China*

<sup>f</sup> *NOAA/National Hurricane Center, Miami, Florida*

(Manuscript received 18 October 2022, in final form 5 May 2023, accepted 11 May 2023)

**ABSTRACT:** Eyewall replacement cycles (ERCs) in tropical cyclones (TCs) are generally associated with rapid changes in TC wind intensity and broadening of the TC wind field, both of which can create unique forecasting challenges. As part of the NOAA Joint Hurricane Testbed Project, a new model was developed to provide operational probabilistic guidance on ERC onset. The model is based on the time evolution of TC wind intensity and passive satellite microwave imagery and is named “M-PERC” for Microwave-Based Probability of Eyewall Replacement Cycle. The model was initially developed in the Atlantic basin but is found to be globally applicable and skillful. The development of M-PERC and its performance characteristics are described here, as well as a new intensity prediction model that extends previous work. Application of these models is expected to contribute to a reduction of TC intensity forecast error.

**KEYWORDS:** Hurricanes/typhoons; Intensification; Operational forecasting; Probability forecasts/models/distribution

## 1. Introduction

The phenomenon of eyewall replacement cycles (ERCs) in tropical cyclones (TCs), in which a secondary outer eyewall forms and eventually replaces the original inner eyewall, is well documented (e.g., Wang et al. 2019; Zhu and Yu 2019, and references therein). ERCs are not just an academic curiosity though, as they generally cause rapid fluctuations in intensity (i.e., rotational wind speed) and a rapid broadening of the TC wind field (Sitkowski et al. 2011, 2012; Kossin and Sitkowski 2012; Rozoff et al. 2012). The former introduces substantial challenges to intensity forecasting and the latter can quickly increase the risk of other TC hazards such as the extent of wind damage and coastal storm surge. One of the challenges of forecasting during an ERC is that they often occur in an environment favorable for TC intensification but usually cause transient and sometimes rapid weakening, which often results in large intensity forecast errors (Kossin and DeMaria 2016). Providing forecasters with information on if and when an ERC begins has the potential to lower these errors.

There is a model presently in operations at the U.S. National Hurricane Center (NHC), called the Probability of Eyewall Replacement Cycle (PERC) model, that provides probability-of-ERC forecasts out to 48-h lead time in the Atlantic basin (Kossin and Sitkowski 2009, hereafter KS09). The PERC model is based on real-time present and forecasted environmental

conditions as well as predictors derived from geostationary satellite infrared sensors. The satellite-based predictors are designed to provide some information about the cloud structure around the TC center and in particular whether a secondary ring of convective clouds may be developing that signals ERC onset. Unfortunately though, infrared sensors do not see through upper-level cirrus clouds well, and TCs typically have a thick cirrus canopy over them that obscures their underlying convective cloud structures in the infrared part of the spectrum. On the other hand, cirrus clouds are essentially transparent to microwave sensors, which makes them well suited for identifying the convective cloud structures of TCs (e.g., Wilheit et al. 1976). The caveat is that microwave sensors generally reside on board low-Earth-orbiting satellites, which cannot provide the same uniformly timed data that geostationary satellites provide, and they suffer from temporal and spatial data gaps that can be large, particularly in the tropics. Still, the microwave data can be used in an operational setting with the understanding that new data may not always be available in time for every 6-hourly operational forecast cycle.

Here we introduce a new model that uses satellite microwave data to produce a probability of ERC onset in tropical cyclones. The model is called the Microwave-Based Probability of Eyewall Replacement Cycle (M-PERC) model, and it is designed to capture the formation of an outer ring of convection (a secondary eyewall) and its subsequent radial contraction toward the primary eyewall.

## 2. Model development

The M-PERC model utilizes output from the Automated Rotational Center Hurricane Eye Retrieval (ARCHER) algorithm (Wimmers and Velden 2010, 2016). The ARCHER

---

Kossin: Retired from NOAA.

---

Corresponding author: James Kossin, jpkossin@wisc.edu

DOI: 10.1175/WAF-D-22-0178.1

© 2023 American Meteorological Society. This published article is licensed under the terms of the default AMS reuse license. For information regarding reuse of this content and general copyright information, consult the AMS Copyright Policy ([www.ametsoc.org/PUBSReuseLicenses](http://www.ametsoc.org/PUBSReuseLicenses)).

Brought to you by NOAA Central Library | Unauthenticated | Downloaded 08/02/23 01:45 PM UTC

algorithm was primarily designed to locate the center of a TC by identifying convective rings and spirals and brightness temperature gradients in 85–92-GHz passive microwave imagery. In TCs with an eye (and thus an eyewall), the algorithm produces a “ring score,” which measures the best fit of the gradients of the eyewall to the shape of a circle. It essentially identifies ring-like convective features, and scores them by how circularly symmetric they are. For the present application of identifying secondary outer eyewalls, the ARCHER ring scores were calculated every 6 km along a radial extending outward from TC center to 200 km, and the resulting radial profile of ring scores was interrogated for secondary maxima.

M-PERC is a statistical model based on logistic regression, which provides a probability of an outcome in a binary classification event based on some set of scalar-valued predictors. In this case, the binary classification of interest is whether or not ERC onset is occurring. The occurrence of ERC onset events was determined similarly to *KS09* (section 2), through visual inspection of microwave imagery, radar imagery, and aircraft data. *KS09* considered secondary eyewall formation (SEF) as a logical antecedent to ERC onset, with the understanding that SEF can occur without leading to an ERC. SEF was identified in the microwave imagery by the appearance of an outer ring of convection that is clearly separated from the primary eyewall convective ring, and forms at least 75% of a complete circle. Identifying SEF from land-based or airborne radar imagery was performed similarly, while identifying SEF from aircraft flight-level tangential wind profiles was based on identification of a persistent secondary maximum outside of the primary eyewall. Whereas *KS09* considered all SEF events regardless of whether they led to an ERC event, here we only consider cases of SEF that lead to an ERC, and we distinguish this by replacing “SEF” with “ERC onset.”

The model was developed using 1787 profiles from 47 Atlantic TCs over the period 1999–2011. Within this period, there were 84 ERC onset events.

To derive scalar-valued regression predictors from the ARCHER ring-score profiles, principal component analysis (PCA) was applied to the set of 1787 profiles to produce a set of loading patterns/profiles [also known as empirical orthogonal functions (EOFs)] and the principal components (or weighting coefficients) were then used as potential predictors. The ring-score profiles were normalized at each radius prior to PCA so that ring-score variability is more constant between the primary eyewall region, where the variability tends to be large and concentrated, and the regions outside where variability is generally smaller and less radially confined. The outer region is where secondary eyewalls can form over a broad range of distance from TC center.

The first three leading loading profiles (EOFs) of the PCA are shown in Fig. 1, which demonstrates the ability of the EOFs to represent circular convective cloud features in the typical region of the primary (inner) eyewall as well as the regions where secondary (outer) eyewalls typically form (*Sitkowski et al. 2011*).

After the PCA, the scalar-valued weights on the EOFs (i.e., the PCs) were added to a set of potential predictors for the logistic regression model. In addition to the formation of a

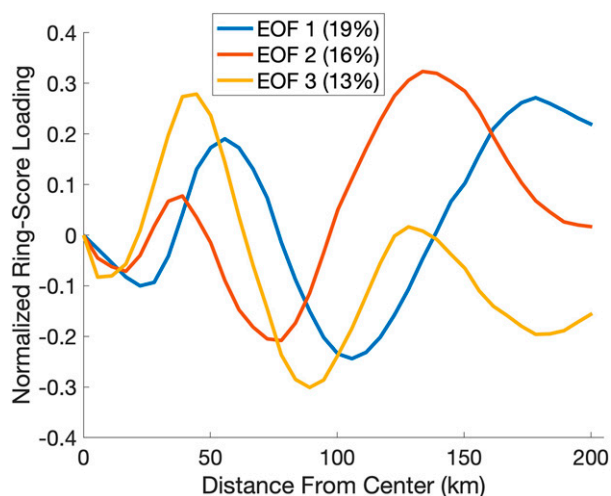


FIG. 1. First three leading loading profiles based on PCA of a set of 1787 ARCHER ring-score profiles. The profiles were normalized prior to PCA by removing the mean of the large set of profiles and dividing by their standard deviation at each radius. Higher-order EOFs have progressively greater radial variation and are not shown here only to maintain the legibility of the figure. The percent variance explained by the first three EOFs is shown in the legend. The first nine EOFs combined explain 90% of the variance.

secondary convective ring, ERCs are generally associated with a subsequent radial contraction of the ring. To capture this process, the change in the PCs over the previous 6, 12, 18, and 24 h were also added to the set of potential predictors. Finally, ERCs are well correlated with intensity and intensity change, and the maximum wind speed and the change in wind speed over the previous 6, 12, 18, and 24 h were added to the set of predictor candidates. More intense TCs are more likely to undergo an ERC (e.g., *KS09*), and ERCs usually form during intensification. A backward-stepwise regression procedure was applied to the large set of predictor candidates to select the most useful predictors, and the final M-PERC model uses the 18 selected predictors shown in Table 1 to produce a probability of ERC onset.

To better separate the effects of the satellite microwave-based predictors (as represented by the PCs) and the TC intensity-based (i.e.,  $V_{\max}$ -based) predictors, a second logistic regression model was formed using only the intensity-based predictors shown in Table 1. The M-PERC output displays the probability from both the full model based on the 18 predictors and the model based only on the three intensity-based predictors. This provides information on whether the convective cloud presentation, as represented by the evolution of the PCs, is more or less likely to represent an ERC onset event than the intensity and intensity changes alone would have suggested. The reduced three-predictor model can be considered as a representation of ERC onset probability climatology as defined solely by intensity and intensity evolution, and provides a baseline for comparison with the full model.

The M-PERC model was designed for operational use and incorporates real-time current and previous intensity (operational or “working” best track) estimates. Microwave data

TABLE 1. List of M-PERC predictors, as selected by a backward-stepping procedure. The PC-based predictors represent the microwave-based contribution to the model, and the  $V_{\max}$ -based predictors represent the intensity-based contributions.

Predictor	Description
PC3	PC 3
PC5	PC 5
PC8	PC 8
PC1-12	12-h change in PC 1
PC2-06	6-h change in PC 2
PC2-18	18-h change in PC 2
PC3-06	6-h change in PC 3
PC3-12	12-h change in PC 3
PC3-18	18-h change in PC 3
PC3-24	24-h change in PC 3
PC4-18	18-h change in PC 4
PC5-18	18-h change in PC 5
PC7-24	24-h change in PC 7
PC9-12	12-h change in PC 9
PC9-24	24-h change in PC 9
$V_{\max}$	Current wind intensity
$V_{\max}$ -12	12-h change in $V_{\max}$
$V_{\max}$ -18	18-h change in $V_{\max}$

from polar-orbiting satellites are available regularly, but satellite data swaths that capture an adequate portion of a traveling TC become available more irregularly. During the life of a TC, M-PERC is designed to update whenever a new microwave pass provides adequate coverage to provide an ARCHER ring-score profile. When a new microwave pass becomes available, the predictors are calculated and interpolated backward in time to 1-hourly in UTC time. This way the M-PERC output is available for every hour during the lifetime of a TC and will always fall on a synoptic or forecast cycle time. Because of the rarity of ERC prior to a TC reaching  $33 \text{ m s}^{-1}$  (hurricane intensity), M-PERC provides zero probability until a TC reaches hurricane intensity. A full 24 h of previous data is required to provide a probability at any forecast time (because of predictor PC3-24 in Table 1), but this can only affect M-PERC if a TC reaches hurricane strength in less than 24 h from genesis, which is unlikely.

The M-PERC model was developed using data from Atlantic storms and was originally intended to be applied to that basin alone, but during routine operational testing, it was found to perform well in every TC basin. This suggests that the microwave evolution of storms shares some common behaviors among the regions, and the principal component predictors are not highly sensitive to the known differences in average storm size among the basins (e.g., Chavas et al. 2016), perhaps because of the smoothed nature of the loading patterns that emerge from PCA. It may be worthwhile to develop M-PERC analogs in other basins, and these may be expected to perform better in their respective basins. The following section discusses the Atlantic-based model performance in several basins. As noted above, the model is routinely applied in real time to all the TC-producing ocean basins. Here we just look at examples from the North Atlantic and eastern and western North Pacific.

### 3. Estimating model performance

Objectively quantifying operational M-PERC model skill is challenging due to the somewhat subjective nature of what comprises ERC onset (and the details of its subsequent evolution). Deciding whether an ERC occurred in real time—often with limited microwave satellite passes, land-based radar, or aircraft penetrations that capture the TC core region—is usually performed subjectively “on-the-fly” by forecasters, and even determining ERC onset in postanalysis is at least partly subjective. At times, a forecaster may explicitly mention ERC onset in a forecast discussion, and these can be used to measure model performance, but even in these cases, determining the actual time of ERC onset within the 6-hourly forecast cycle is imprecise. With this understanding that measuring skill objectively and exactly is not a realistic expectation (as it could be, for example, for a track or intensity forecast model), here we provide some estimates of M-PERC model performance using the Brier skill score (Brier 1950) and less quantitatively via a case study.

As noted above, the M-PERC model runs in real time and consequently the TC wind intensity information used as input comprises estimates known as working best-track data. These intensity estimates are based on information available during the time of the operational forecast cycle, and they are often updated after the fact to include other information that may have become available. The postanalysis estimates also benefit from expert judgement of the forecasters and this ultimately leads to the final best-track data, which represents the most accurate intensity estimates. The Brier skill scores presented here may be affected by intensity estimation errors and are likely to present a conservative skill assessment of the model.

We begin with independent testing of the M-PERC model on North Atlantic TCs. The Brier skill scores computed here use a climatological probability of 13% based on the 1999–2011 Atlantic training data (cf. KS09). Over the independent testing period 2012–20, we have 48 ERC events in 24 Atlantic hurricanes, resulting in a Brier skill score of 35% for the full M-PERC model compared to 27% for the model using only intensity-based predictors. The difference between the skill of the intensity-based model and the full model demonstrates the contribution of the satellite data, which increases skill by about 30% (from 27% to 35%).

In the eastern North Pacific, we have a more limited sample of 23 ERC events in 14 storms over the period 2017–21. Within this sample, the climatological probability of ERC onset is 11%, which is slightly lower than the Atlantic climatology of 13%. Applying the model in this basin gives Brier skill scores of 41% and 33% for the full model and intensity-based model, respectively. Here the addition of the satellite data to the intensity data increases skill by about 24%.

Our present samples in the remaining basins are too small to perform robust skill assessments, but with an understanding of this caveat we formed a sample in the western North Pacific during the year 2020. The climatological value from this small sample is 26%, which suggests that ERC onset is generally more likely in this basin (compared with 13% and 11% in the Atlantic and eastern North Pacific, respectively). Using this

value, the Brier skill scores for the full M-PERC model and the intensity-based model are 31% and 20%, respectively.

Another way to identify the contribution of the satellite data to the M-PERC model is to use the intensity-based-only model output as the climatology instead of fixed values. When we follow this procedure in the North Atlantic independent testing sample, the Brier skill score is 11%, which again indicates that the satellite data measurably increases model skill. Following this procedure in the eastern and western North Pacific, the Brier skill scores are 13% in both basins.

For our case study, we use 2022 North Atlantic Hurricane Ian (Bucci et al. 2023). The operational output of the M-PERC model displays three panels that evolve in time (Fig. 2). The microwave ring-score profiles for each time are shown as a standard Hovmöller diagram with time increasing downward. The M-PERC probabilities of ERC onset for each time are displayed with the simplified model probabilities that are based only on intensity and intensity change metrics (i.e., with no satellite information). The intensity evolution is shown using operational or working best track from the National Hurricane Center. Annotated arrows and text show the microwave response to the complete ERC observed in Hurricane Ian.

The formation of a nascent secondary eyewall and the associated moat feature between the primary and secondary eyewalls occurs during 26 September. A more detailed discussion of these features is found in KS09. The subsequent symmetrization, convective intensification, and contraction of the secondary eyewall is observed during 27 September, and the ERC completes on 28 September. ERC completion is defined here as in Kossin and Sitkowski (2012): when there is no longer an observed inner local wind maximum. M-PERC probabilities of ERC onset remain mostly constant and near zero until around 0600 UTC on 27 September and increase rapidly to about 60% in the next 6 h. After this time, the lack of symmetric convective features outside of the contracting secondary eyewall drives the probabilities down to near zero again. This same lack of convective features also keeps the M-PERC probabilities below the probabilities based solely on intensity. The operational best track intensity evolution demonstrates the well-known effects of an ERC on intensity (e.g., Willoughby et al. 1982; Sitkowski et al. 2011; Kossin and DeMaria 2016). As the secondary eyewall contracts, the intensification rate decreases abruptly, causing an inflection point. In the case of Hurricane Ian, this decrease was large enough to result in a transition from a period of intensification to a short period of weakening and a longer period of steady state. After this, a period of rapid intensification follows as the new (and much larger) primary eyewall intensifies.

M-PERC model output is available in real time for tropical cyclones in all basins at the URL [http://tropic.ssec.wisc.edu/real-time/archerOnline/web/index\\_erc.shtml](http://tropic.ssec.wisc.edu/real-time/archerOnline/web/index_erc.shtml). An archive of M-PERC output that can be used to consider other case studies is also found at the link.

#### 4. Intensity evolution climatology during ERCs

The M-PERC model provides a probability that an ERC is underway. A logical next question for a forecaster is how best

to adjust the available intensity forecast guidance to account for this. As described in Kossin and DeMaria (2016) and noted above, one of the major challenges of forecasting during an ERC is that they generally occur in an environment favorable for continued TC intensification, but usually cause a transient decrease in intensification rate and, in many cases, a decrease in intensity. An important tool for forecasting TC intensity change in the Atlantic is the Statistical Hurricane Intensity Prediction Scheme (SHIPS). Because SHIPS provides intensity change forecasts based primarily on a hurricane's ambient environmental conditions, SHIPS errors can be large during ERCs (Kossin and DeMaria 2016). At high enough spatial resolutions, numerical models can simulate ERCs that cause transient intensification rate changes (e.g., Nolan et al. 2013; Molinari et al. 2019), but in an operational setting, this is not of much practical use. Within a 6-h forecast cycle, the timing of the simulated ERC would need to coincide within an hour or two of the observed ERC, which is not a realistic expectation. If the timing of the simulated ERC does not coincide very closely with the actual ERC, the simulated intensity guidance is likely to introduce greater errors than if an ERC was not simulated at all. This lack of effective statistical and numerical intensity guidance during ERCs is the motivation for this section, which introduces an extended version of the ERC intensity-change model described in Kossin and DeMaria (2016).

Kossin and DeMaria (2016) formed a model based on ERC intensity climatology that could be used as a temporary replacement for SHIPS, similar to the application of the “decay-SHIPS” (D-SHIPS) model while storms are over land (Kaplan and DeMaria 1995; DeMaria et al. 2005). They based their climatology on 19 Atlantic ERC events. Given the small sample, they did not stratify the events by intensity at ERC onset, but it was understood that this was not optimal. The motivation for such a stratification stems from the observation that the decrease in intensification rate associated with ERCs is a function of intensity at ERC onset, with larger intensification rate decreases in stronger storms (Kossin 2015, his Fig. 3). In fact, Kossin (2015) showed that ERCs that occur during the earlier weaker part of the TC lifetime can sometimes coincide with continued, albeit reduced, intensification. Alternatively, ERCs that occur near the lifetime peak intensity of the TC almost always coincide with a change in sign of the intensification rate (i.e., weakening intensity).

Here we exploit our larger sample of ERC events to form three separate intensity-change climatologies based on Saffir–Simpson category at the time of ERC onset. These are summarized in Fig. 3. The climatological time evolution is based on the observed inflection point of the intensification rate relative to the observed onset of an ERC event. The inflection point was identified using HURDAT2 best-track intensity data (Landsea and Franklin 2013). As seen in Fig. 3, ERC events in all hurricanes, regardless of intensity, coincide with a mean decrease in intensification rate, but the decrease becomes substantially greater with higher Saffir–Simpson category. Weaker [category 1–2; 64–95 kt (1 kt  $\approx$  0.51 m s<sup>-1</sup>)] hurricanes coincide with a transition from intensifying to roughly steady state and, in some cases, continued but reduced

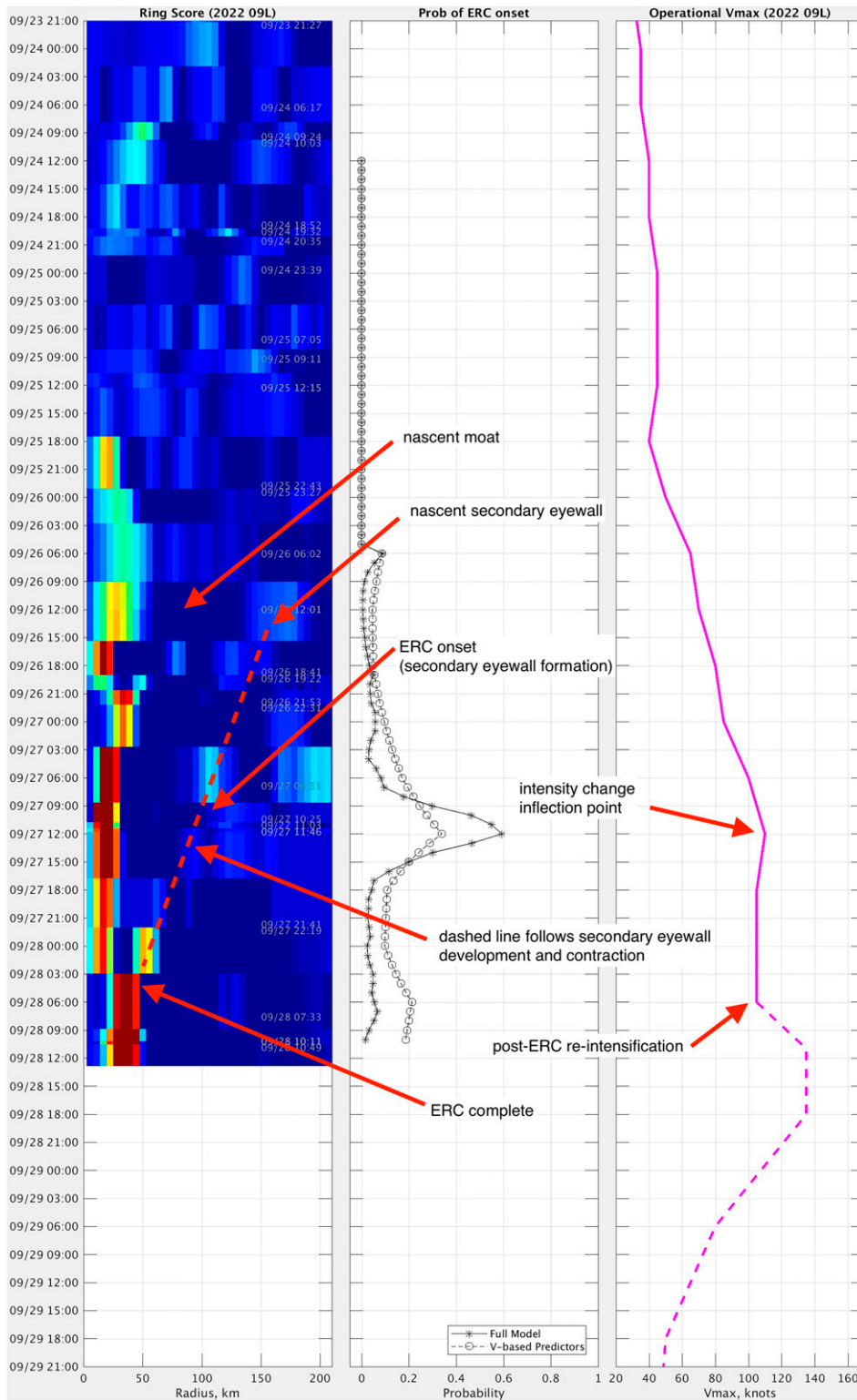


FIG. 2. Operational M-PERC model output during North Atlantic Hurricane Ian (2022). (left) A Hovmöller diagram of ARCHER microwave ring score profiles. Time (displayed as UTC month/day hour:minute) increases downward, and radius indicates distance (km) from storm center. (center) The probability of ERC onset based only on intensity and intensity change (open circles) and based on the full M-PERC model (asterisks), which also incorporates the microwave-based predictors. (right) The operational best track estimates of intensity (kt).

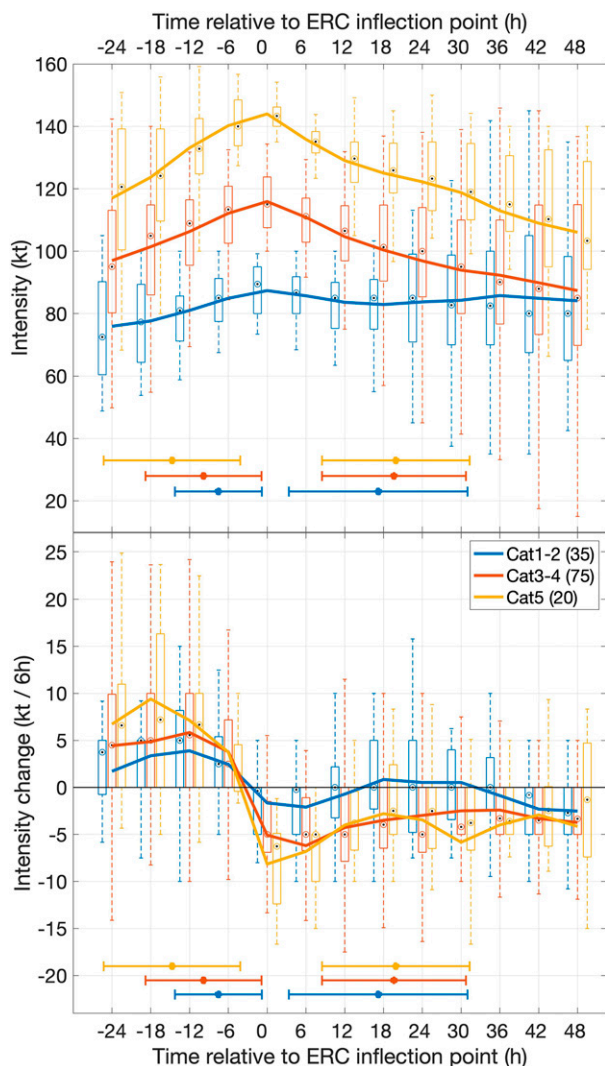


FIG. 3. Climatology of the evolution of (top) intensity and (bottom) intensity change during Atlantic hurricane ERC events. The climatologies are separated by Saffir–Simpson category. The number of events that the climatologies are based on is shown in parentheses in the legend. Boxplots show the interquartile range, the open circles show the median, and the whiskers show the 99% range. Superimposed on the box-and-whisker plots are lines connecting the mean values. The horizontal bars represent the onset and completion times of the ERC events relative to the intensity change inflection point. The dots show the means, and the error bars show  $\pm 1$  standard deviation.

intensification. Category 3–4 (96–136 kt) hurricanes exhibit a larger reduction in intensification rate and generally experience a transient weakening of about  $5 \text{ kt } (6 \text{ h})^{-1}$ . Category 5 (137 kt and higher) hurricanes exhibit the most dramatic change from an intensification rate of about  $+10 \text{ kt } (6 \text{ h})^{-1}$  just prior to ERC onset to an eventual weakening of about  $10 \text{ kt } (6 \text{ h})^{-1}$ .

On average, the first signs of ERC onset occur, respectively, about 7, 10, and 15 h prior to the intensification rate inflection point in category 1–2, 3–4, and 5 hurricanes (points on the

horizontal bars in Fig. 3). On average, the ERC has completed, respectively, about 17, 19, and 19 h after the intensification rate inflection point in category 1–2, 3–4, and 5 hurricanes. As noted above, ERC completion is defined here as in Kossin and Sitkowski (2012): when there is no longer an observed inner local wind maximum.

Here we summarize and simplify the intensity-change climatology in a way that may be used in an operational forecasting setting:

- 1) The behavior of the M-PERC model suggests ERC onset is occurring. This would generally be based on a persistent increase in probability, and signs of secondary eyewall formation and contraction in the M-PERC Hovmöller diagram. Forecaster confidence in secondary eyewall formation may also depend on other lines of evidence (e.g., aircraft- or ground-based radar, aircraft flight-level wind data, the environmental-based PERC model, etc.)
- 2) If confidence is high enough, the intensity forecast based on SHIPS and other numerical guidance can be temporarily modified.
  - (i) If the current intensity is category 1–2, the climatology suggests reducing the intensification rate to about zero over the next 6–12 h and holding intensity steady for about 18 h after that.
  - (ii) If the current intensity is category 3–4, the climatology suggests reducing the intensification rate to about  $-5 \text{ kt } (6 \text{ h})^{-1}$  over the next 12 h and then increasing the rate to about  $-3 \text{ kt } (6 \text{ h})^{-1}$  over the next 18 h.
  - (iii) If the current intensity is category 5, the climatology suggests reducing the intensification rate to about  $-8 \text{ kt } (6 \text{ h})^{-1}$  over the next 15 h and then increasing the rate to about  $-3 \text{ kt } (6 \text{ h})^{-1}$  over the next 18 h.

## 5. Summary

Here we introduced a new model that provides a real-time probability of ERC onset. The model output is globally operationally available online and is based on a suite of predictors used as input to a logistic regression model. A subset of the predictors is based only on operational intensity and past intensity change estimates, and another subset is based on real-time satellite microwave imagery. The microwave-based predictors are based on the loading functions of a principal component analysis of microwave ring-score profiles.

The model output can be used to provide predictive information regarding the potential fluctuations of intensity that may occur during an ERC. An additional model is introduced that can help to quantify these potential changes in intensity. This model extends the model introduced by Kossin and DeMaria (2016). The operational application of these two models is expected to contribute to the broader goal of decreasing operational intensity estimates.

*Acknowledgments.* This work was funded under Federal Grant Award NA19OAR4590132, “Upgrades to the M-PERC and PERC Models to Improve Short Term Tropical Cyclone

Intensity Forecasts,” Federal Grant Award NA15OAR4590197, “Improved Eyewall Replacement Cycle Forecasting Using a Modified Microwave-Based Algorithm (ARCHER),” and Federal Grant Award NA20NES4320003, “Direct integration of JPSS observations into tropical cyclone surface wind structure retrievals using deep learning.”

*Data availability statement.* Data may be provided, on reasonable request, from the authors.

## REFERENCES

- Brier, G. W., 1950: Verification of forecasts expressed in terms of probability. *Mon. Wea. Rev.*, **78**, 1–3, [https://doi.org/10.1175/1520-0493\(1950\)078<0001:VOFEIT>2.0.CO;2](https://doi.org/10.1175/1520-0493(1950)078<0001:VOFEIT>2.0.CO;2).
- Bucci, L., L. Alaka, A. Hagen, S. Delgado, and J. Beven, 2023: Tropical cyclone report: Hurricane Ian (AL092022). NHC Tech. Rep., 72 pp., [https://www.nhc.noaa.gov/data/tcr/AL092022\\_Ian.pdf](https://www.nhc.noaa.gov/data/tcr/AL092022_Ian.pdf).
- Chavas, D. R., N. Lin, W. Dong, and Y. Lin, 2016: Observed tropical cyclone size revisited. *J. Climate*, **29**, 2923–2939, <https://doi.org/10.1175/JCLI-D-15-0731.1>.
- DeMaria, M., M. Mainelli, L. K. Shay, J. A. Knaff, and J. Kaplan, 2005: Further improvements to the Statistical Hurricane Intensity Prediction Scheme (SHIPS). *Wea. Forecasting*, **20**, 531–543, <https://doi.org/10.1175/WAF862.1>.
- Kaplan, J., and M. DeMaria, 1995: A simple empirical model for predicting the decay of tropical cyclone winds after landfall. *J. Appl. Meteor.*, **34**, 2499–2512, [https://doi.org/10.1175/1520-0450\(1995\)034<2499:ASEMFP>2.0.CO;2](https://doi.org/10.1175/1520-0450(1995)034<2499:ASEMFP>2.0.CO;2).
- Kossin, J. P., 2015: Hurricane wind–pressure relationship and eyewall replacement cycles. *Wea. Forecasting*, **30**, 177–181, <https://doi.org/10.1175/WAF-D-14-00121.1>.
- , and M. Sitkowski, 2009: An objective model for identifying secondary eyewall formation in hurricanes. *Mon. Wea. Rev.*, **137**, 876–892, <https://doi.org/10.1175/2008MWR2701.1>.
- , and —, 2012: Predicting hurricane intensity and structure changes associated with eyewall replacement cycles. *Wea. Forecasting*, **27**, 484–488, <https://doi.org/10.1175/WAF-D-11-00106.1>.
- , and M. DeMaria, 2016: Reducing operational hurricane intensity forecast errors during eyewall replacement cycles. *Wea. Forecasting*, **31**, 601–608, <https://doi.org/10.1175/WAF-D-15-0123.1>.
- Landsea, C. W., and J. L. Franklin, 2013: Atlantic hurricane database uncertainty and presentation of a new database format. *Mon. Wea. Rev.*, **141**, 3576–3592, <https://doi.org/10.1175/MWR-D-12-00254.1>.
- Molinari, J., J. A. Zhang, R. F. Rogers, and D. Vollaro, 2019: Repeated eyewall replacement cycles in Hurricane Frances (2004). *Mon. Wea. Rev.*, **147**, 2009–2022, <https://doi.org/10.1175/MWR-D-18-0345.1>.
- Nolan, D. S., R. Atlas, K. T. Bhatia, and L. R. Bucci, 2013: Development and validation of a hurricane nature run using the joint OSSE nature run and the WRF model. *J. Adv. Model. Earth Syst.*, **5**, 382–405, <https://doi.org/10.1002/jame.20031>.
- Rozoff, C. M., D. S. Nolan, J. P. Kossin, F. Zhang, and J. Fang, 2012: The roles of an expanding wind field and inertial stability in tropical cyclone secondary eyewall formation. *J. Atmos. Sci.*, **69**, 2621–2643, <https://doi.org/10.1175/JAS-D-11-0326.1>.
- Sitkowski, M., J. P. Kossin, and C. M. Rozoff, 2011: Intensity and structure changes during hurricane eyewall replacement cycles. *Mon. Wea. Rev.*, **139**, 3829–3847, <https://doi.org/10.1175/MWR-D-11-00034.1>.
- , —, —, and J. Knaff, 2012: Hurricane eyewall replacement cycles and the relict inner eyewall circulation. *Mon. Wea. Rev.*, **140**, 4035–4045, <https://doi.org/10.1175/MWR-D-11-00349.1>.
- Wang, H., Y. Wang, J. Xu, and Y. Duan, 2019: The axisymmetric and asymmetric aspects of the secondary eyewall formation in a numerically simulated tropical cyclone under idealized conditions on an  $f$  plane. *J. Atmos. Sci.*, **76**, 357–378, <https://doi.org/10.1175/JAS-D-18-0130.1>.
- Wilheit, T. T., J. S. Theon, W. E. Shenk, L. J. Allison, and E. B. Rodgers, 1976: Meteorological interpretations of the images from the nimbus 5 electrically scanned microwave radiometer. *J. Appl. Meteor.*, **15**, 166–172, [https://doi.org/10.1175/1520-0450\(1976\)015<0166:MIOTIF>2.0.CO;2](https://doi.org/10.1175/1520-0450(1976)015<0166:MIOTIF>2.0.CO;2).
- Willoughby, H. E., J. A. Clos, and M. G. Shoreibah, 1982: Concentric eye walls, secondary wind maxima, and the evolution of the hurricane vortex. *J. Atmos. Sci.*, **39**, 395–411, [https://doi.org/10.1175/1520-0469\(1982\)039<0395:CEWSWM>2.0.CO;2](https://doi.org/10.1175/1520-0469(1982)039<0395:CEWSWM>2.0.CO;2).
- Wimmers, A. J., and C. S. Velden, 2010: Objectively determining the rotational center of tropical cyclones in passive microwave satellite imagery. *J. Appl. Meteor. Climatol.*, **49**, 2013–2034, <https://doi.org/10.1175/2010JAMC2490.1>.
- , and —, 2016: Advancements in objective multi-satellite tropical cyclone center fixing. *J. Appl. Meteor. Climatol.*, **55**, 197–212, <https://doi.org/10.1175/JAMC-D-15-0098.1>.
- Zhu, X.-S., and H. Yu, 2019: Environmental influences on the intensity and configuration of tropical cyclone concentric eyewalls in the western North Pacific. *J. Meteor. Soc. Japan*, **97**, 153–173, <https://doi.org/10.2151/jmsj.2019-008>.